Comparison of Two Magnetic Saturation Models of Induction Machines and Experimental Validation

Oleh Kiselychnyk, *Member, IEEE*, Marc Bodson, *Fellow, IEEE*, and Jihong Wang, *Senior Member, IEEE*

***Abstract*—This paper develops a systematic comparison of two nonlinear models of induction machines in magnetic saturation using stator and rotor currents as state variables. One of the models accounts for dynamic cross-saturation effects, whereas the other neglects them. Analytic derivations yield an explicit description of the difference between the models showing that differences can only be observed through transient responses in the saturated region. To refine the comparison, and exclude conditions in the linear magnetic region, the dynamics of self-excited induction generators around stable operating points is analyzed. Unexpected and interesting features of the models are revealed through their linearization in the reference frame aligned with the stator voltage vector, followed by computation of the transfer functions from perturbations to state deviations. The analysis predicts a slower exponential convergence of the simplified model compared to the full model, despite very close responses in the initial period. The comparison is validated via thorough experiments and simulations. This paper provides experimental evidence of the higher accuracy of the full model for transients deep into the saturated region. For realistic operating conditions, the difference is found to be rather small, and often comparable to the steady-state error caused by inaccuracies in the parameters.**

***Index Terms*—Electric machines, generators, induction machines, nonlinear dynamical systems, self-excitation.**

I. Introduction

THEORETICAL approaches for the analysis of induction machines are well established. A generalized two-phase model of an induction machine of fifth order assuming linear magnetics is the most widely used. However, induction machines often operate in the saturated region of the magnetization curve, where their behavior differs significantly from the model with linear magnetics.

Models accounting for magnetic saturation are typically derived from the model with linear magnetics by incorporating into the model a static function describing the magnetic nonlinearity. Features of the models depend significantly on the choice of state variables [1], [2]. The most widely used model is the model with stator and rotor currents as state coordinates [1], [3]–[6]. Another choice consists in choosing stator and rotor flux linkages. In the first case, it is necessary to differentiate the magnetizing inductance function with respect to time, leading to terms in the model known as dynamic cross-saturation effects. A physical explanation of dynamic cross-saturation was provided in [7]. In the second case, differentiation is avoided, but the corresponding model is more difficult to use for simulation and analysis, because the unsaturated magnetizing flux cannot be determined explicitly from the state vector. Models with a mixed choice of state variables (stator currents with rotor flux linkages as well as other combinations) have also found applications in simulations of saturated induction machines [1], [8], [9]. These models also have terms associated with dynamic cross-saturation, although the effect of neglecting these terms can be significantly different than for the models using only current variables.

The saturated induction machine models are well validated experimentally based on voltage build-up processes in self-excited generating mode [1], [2], [6], [9]–[11], switching of a resistive load to the self-excited induction generator (SEIG) [11], and switch-off with reclosing transients of an induction motor with parallel reactive power compensation [3], [10]. In [10], the state-space model with stator and rotor currents is also experimentally validated for steady-state operation of an induction motor drive fed by a current source inverter and by a parallel resonant inverter.

In contrast, many authors have used a simplified model with the currents as state variables that neglects the dynamic cross-saturation terms [12], [13]. The model can be obtained simply by replacing the magnetizing inductance in the model with linear magnetics by a nonlinear function of the magnetizing current amplitude. The simplified model is inconsistent with generally accepted principles of electric machine modeling. However, the model has proved valuable and is also well supported experimentally [14]–[18].

The objective of this paper is to explore differences between the model accounting for dynamic cross-saturation effects and the model neglecting these effects, in both cases with the currents as state variables. These models will be referred to as the *full model* and the *simplified model*, respectively. Note that both models account for cross-saturation terms known as steady-state cross-saturation terms, since the magnetizing inductance

Manuscript received March 3, 2016; revised June 8, 2016; accepted July 8, 2016. Date of publication September 13, 2016; date of current version December 9, 2016. This work was supported by the Engineering and Physical Sciences Research Council, U.K., under Grant EP/L014211/1 and Grant EP/L019469/1.

O. Kiselychnyk and J. Wang are with the School of Engineering, University of Warwick, Coventry, CV4 7AL, U.K (e-mail: O.Kiselychnyk@warwick.ac.uk; jihong.wang@warwick.ac.uk).

M. Bodson is with the Department of Electrical and Computer Engineering, University of Utah, Salt Lake City, UT 84112 USA (e-mail: bodson@eng.utah.edu).

Color versions of one or more of the figures in this paper are available online at http://ieeexplore.ieee.org.

Digital Object Identifier 10.1109/TIE.2016.2608766

is a function of the currents in both axes of the two phase models. Thus, the models only differ in the dynamic cross-saturation terms which are zero in steady-state.

Since experiments have shown that the difference between the models is, in many cases, of the same order of magnitude as the steady-state errors between the models and the experimental data, due to inaccuracies in the machine's parameters and in the magnetization curve approximation, we seek in this paper the direct validation of both models from experimental data. Although we review below previous works in this direction which contain an explicit comparison of the full and simplified models, these papers do not use experimental data as the criterion by which the relative accuracy of one model is compared to the other. Previous work also includes models with a combination of the currents and fluxes as state coordinates, for which simplified versions can also be obtained.

In [19] and [20], the results of simulation of the full and simplified models for an induction motor starting with a voltage sufficient to reach magnetic saturation and with models using the currents as states variables are reported. A comparison is also presented for the models with fluxes and currents as state variables in the cases of the motor start [20] and reverse [21], [22]. Conclusions are drawn that the simplified currents model gives incorrect predictions based on the observation that the simulation of the full model resembles the transients of the model with linear magnetics only with reduced values of the torque peaks [19], [20], whereas the simplified model predicts lower torque peaks that are also significantly shifted in time. However, the stator currents of both models are in good agreement [19]. Unfortunately, experimental curves of the transient torque for the motor starting and reverse processes corresponding to the simulation cases are not presented in [19]–[22]. Note that a clear difference between the models could only be seen during very fast mechanical transients (in [19]–[22], the time periods are less than 0.25 s) when accurate transient torque measurements are quite difficult [3]. In the case of the mixed current-flux linkage models which require time derivative of the inverse of the generalized magnetizing inductance [20], the difference in simulated behaviors of the full and simplified models is reported as negligible. Based on these conclusions, the world-recognized commercial transient simulation package PLECS uses such a model (with stator currents and magnetizing flux linkages as state variables), ignoring the dynamic cross-saturation for numerically efficient simulation of saturated induction machines [23]. In contrast, this paper considers the model with current variables only, for which the omission of dynamic cross-saturation causes greater differences in responses between the models.

Experimentally validated results including a comparison of the full and simplified models are presented in [20] and [11] for the induction machine in self-excited generating mode. Conclusions are drawn on the incorrectness of the simplified currents model [20] based on the comparison of the voltage build-up transients, similarly to the full model validation in [1] and [10]. However, these transients are significantly affected by the magnetizing inductance curve for low currents (ascending part). Experimental determination of the magnetizing inductance for this region is less accurate than for the saturation region (descending part) and requires specific no load motor tests with slip compensation. The magnetization curve approximation could favor one of the models since both of them are very sensitive to its parameters. Another problem influencing the accuracy of the voltage build-up simulation is that the initial state vectors of the models are chosen heuristically because of the problem of the measurement of the residual magnetization. Note that for the case of the SEIG voltage build-up, Levi [20] also reports excellent agreement between the full and simplified mixed current-flux linkage models of the inversed generalized magnetizing inductance type. Hallenius *et al.* [11] experimentally validate the full currents model for voltage build-up and load switching, but the difference between the responses of the models is shown only for stator current magnitudes and without corresponding experimental data.

This paper presents a systematic comparison of the full and simplified models of the induction machine using current variables. It does not contradict the general conclusions of [11] and [19]–[22] but it adds new insights to the dynamic cross-saturation validation through experiments that avoid inaccuracies of the previous investigations. This paper includes the theoretical results of [24], updated based on the recent methodology from [25] that explains the similarity of the models at the beginning of the transients. Compared to [24], improvements were made by testing a different SEIG and the accuracy of the results was enhanced through the following:

1) measurements of all three line-to-line voltages instead of a single one, which enables the reconstruction of an instantaneous voltage magnitude estimate and a clearer representation of voltage magnitude perturbations;
2) investigation of the voltage deviations caused by the velocity, capacitance and load perturbations instead of only a load change in [24], including the determination of conditions maximizing the difference;
3) additional tests using periodic voltage perturbations caused by periodic capacitance and velocity changes;
4) incorporation of measured velocities in the simulations;
5) reduction of the influence of inaccurate machine parameters by selecting operating conditions providing small and comparable steady-state errors;
6) a new approach for the determination of the saturated magnetizing inductance based on experimental steady-state self-excited operation data.

The investigation provides clear experimental evidence of the higher accuracy of the full model for transient behavior deeply in the saturated region. For operating conditions closer to the onset of saturation, the difference between the models is found to be rather small.

II. Models of Induction Machines

A. Full Nonlinear Model

The full two-phase model of the induction machine with the currents as state variables in an arbitrary orthogonal reference frame $F-G$ can be put into the form of the nonlinear matrix

differential equation [6]

$$E\dot{X} = FX + BU \tag{1}$$

where

$$X = \left[\, i_{\rm SF}\ i_{\rm RF}\ i_{\rm SG}\ i_{\rm RG} \,\right]^T,\ U = \left[\, U_{\rm SF}\ U_{\rm SG} \,\right]^T,$$

$$E = \begin{bmatrix} E_F & E_{\rm FG} \\ E_{\rm FG} & E_G \end{bmatrix},\ F = \begin{bmatrix} F_1 & -F_2 \\ F_2 & F_1 \end{bmatrix},\ B = \begin{bmatrix} 1\,0\,0\,0 \\ 0\,0\,1\,0 \end{bmatrix}^T,$$

$$E_F = \begin{bmatrix} L_{\sigma\rm S} + L_{\rm MF} & L_{\rm MF} \\ L_{\rm MF} & L_{\sigma\rm R} + L_{\rm MF} \end{bmatrix},$$

$$E_G = \begin{bmatrix} L_{\sigma\rm S} + L_{\rm MG} & L_{\rm MG} \\ L_{\rm MG} & L_{\sigma\rm R} + L_{\rm MG} \end{bmatrix},$$

$$E_{\rm FG} = \begin{bmatrix} L_{\rm MFG} & L_{\rm MFG} \\ L_{\rm MFG} & L_{\rm MFG} \end{bmatrix},\ F_1 = \begin{bmatrix} -R_S & 0 \\ 0 & -R_R \end{bmatrix},$$

and

$$F_2 = \begin{bmatrix} -\omega_e(L_{\sigma\rm S} + L_M) & -\omega_e L_M \\ (n_p\omega - \omega_e)L_M & (n_p\omega - \omega_e)(L_{\sigma\rm R} + L_M) \end{bmatrix}.$$

In the model, ω_e denotes the angular velocity of the $F-G$ reference frame with respect to the stationary stator frame $A-B$, $U_{\rm SF}$, $U_{\rm SG}$, $i_{\rm SF}$, and $i_{\rm SG}$ are the stator voltages and currents, respectively, $i_{\rm RF}$, $i_{\rm RG}$ are the rotor currents, ω denotes the angular velocity of the rotor, R_S and R_R are the stator and rotor resistances, respectively, $L_{\sigma\rm S}$ and $L_{\sigma\rm R}$ are the stator and rotor leakage inductances, respectively, and n_p is the number of pole pairs. A complete model also includes equations for the position and angular velocity of the motor, but these equations will not be used in this paper.

The nonlinear inductances $L_{\rm MF}$, $L_{\rm MG}$, and $L_{\rm MFG}$ are defined by

$$\begin{aligned} L_{\rm MF} &= L_M + (L - L_M)i_{\rm MF}^2/i_M^2, \\ L_{\rm MG} &= L_M + (L - L_M)i_{\rm MG}^2/i_M^2, \\ L_{\rm MFG} &= (L - L_M)i_{\rm MF}i_{\rm MG}/i_M^2, \end{aligned} \tag{2}$$

where L_M and L are the instantaneous and dynamic magnetizing inductances, respectively, and $i_M = \sqrt{i_{\rm MF}^2 + i_{\rm MG}^2}$ is the magnitude of the magnetizing current with $i_{\rm MF} = i_{\rm SF} + i_{\rm RF}$ and $i_{\rm MG} = i_{\rm SG} + i_{\rm RG}$.

Both magnetizing inductances are static nonlinear functions of the magnetizing current, $L_M = f_1(i_M)$, $L = f_2(i_M)$. The function $L_M = f_1(i_M)$ is obtained as an analytic approximation of the experimental magnetization curve, whereas L is computed from $L_M = f_1(i_M)$ using $L = d(L_M i_M)/di_M$ [6].

B. Simplified Model

The model of induction machine with linear magnetics (derived as (1), but with $L_M = \text{const}$) can be represented as

$$E_L\dot{X} = FX + BU \tag{3}$$

where

$$E_L = \begin{bmatrix} E_{LM} & 0 \\ 0 & E_{LM} \end{bmatrix},\ E_{LM} = \begin{bmatrix} L_{\sigma\rm S} + L_M & L_M \\ L_M & L_{\sigma\rm R} + L_M \end{bmatrix}.$$

If the nonlinear function $L_M = f_1(i_M)$ (the same as for the full model) is incorporated into (3), one obtains the simplified nonlinear model. The simplified model differs from the full model through the terms associated with dL_M/dt. Comparing the models, one finds that the simplified model is the same as the full model, but with L replaced by L_M [6], [20] (note that the reverse is not true).

C. Relationship Between the Models

After substitution into (1), the following equality:

$$\begin{bmatrix} L_{\rm MF} - L_M & L_{\rm MFG} \\ L_{\rm MFG} & L_{\rm MG} - L_M \end{bmatrix} \frac{d}{dt}\left(\begin{bmatrix} i_{\rm MF} \\ i_{\rm MG} \end{bmatrix}\right) = \frac{L - L_M}{i_M}\frac{di_M}{dt}\begin{bmatrix} i_{\rm MF} \\ i_{\rm MG} \end{bmatrix} \tag{4}$$

yields an alternative representation of the full model showing explicitly the difference between the two models

$$E_L\dot{X} = FX + BU - \frac{L - L_M}{i_M}\frac{di_M}{dt}X_M \tag{5}$$

where $X_M = \left[\, i_{\rm MF}\ i_{\rm MF}\ i_{\rm MG}\ i_{\rm MG} \,\right]^T$. The last term is zero if $L = L_M$, in which case both models become the model with linear magnetics and $L_M = \text{const}$. However, the models also become identical when $di_M/dt = 0$. Therefore, a solution of the simplified model (3) for which $i_M = \text{const}$ is also a solution of the full model (1). In other words, both models predict the same steady-state responses in the linear and nonlinear magnetic regions, and the same dynamic responses in the linear region. Any study on the differences between the models requires transient responses with excursions deep enough into magnetic saturation.

To better understand the fundamental differences between the full and simplified models, consider the example of a single winding with current i_M. The total flux linkage Ψ_M satisfies

$$\frac{d\Psi_M}{dt} = v_M - Ri_M \tag{6}$$

where v_M is the voltage applied to the winding and R is the resistance of the winding. L_M and L are defined by

$$L_M = \frac{\Psi_M}{i_M},\quad L = \frac{d\Psi_M}{di_M} = L_M + \frac{dL_M}{di_M}i_M. \tag{7}$$

Using the expression for L in (6), one obtains the equivalent of the full model

$$L\frac{di_M}{dt} = v_M - Ri_M \tag{8}$$

while the simplified model is

$$L_M\frac{di_M}{dt} = v_M - Ri_M. \tag{9}$$

The two models become identical if $L = L_M$, which is the case if L_M is constant, i.e., if Ψ_M is proportional to i_M.

In the case of magnetic saturation and a current i_M in the saturation region, one has $L < L_M$, and therefore

$$\left(\frac{di_M}{dt}\right)_{\rm FULL\ MODEL} > \left(\frac{di_M}{dt}\right)_{\rm SIMPLIFIED\ MODEL} \tag{10}$$

in the initial part of the response to a step in voltage. Thus, transient responses are expected to be faster for the full model and the eigenvalues of its linearized system in the saturation region are expected to be larger in magnitude.

Interesting insights can also be obtained by considering the power absorbed by the winding. In the case of the full model

$$v_M i_M = R i_M^2 + \frac{d\Psi_M}{dt} i_M = R i_M^2 + \frac{dW}{dt} \tag{11}$$

where $W = \int_0^{\Psi_M} i_M(\Psi_M) d\Psi_M$ is the energy stored in the magnetic circuit, and corresponds to the classical definition of the stored magnetic energy [26]. In the case of the simplified model

$$v_M i_M = R i_M^2 + L_M \frac{di_M}{dt} i_M = R i_M^2 + \frac{dW'}{dt} \tag{12}$$

where $W' = \int_0^{i_M} i_M L_M(i_M) di_M$ is again the energy stored in the magnetic circuit, but it does not match the classical definition of stored magnetic energy. Interestingly, the definition in the case of the simplified model corresponds to the so-called *co-energy*, which is a fictitious energy component that is found helpful to compute the torque of electric machines in saturation [26]. In general, $W + W' = \Psi_M i_M$. When in magnetic saturation, $W' > W$, which means that the energy needed to reach a certain flux level is larger for the simplified model than for the full model. Intuitively, this explains the fact that the response of the simplified model should be slower.

This discussion brings up the fact that the simplified model poses a serious conceptual problem since its differential equations are not derived from accepted modeling principles for electromechanical devices. The model involves a concept of stored energy, but the energy has the wrong value. Nevertheless, the impact of this error may be difficult to observe, because the stored magnetic energy is small compared to other energetic components, including the converted energy, and even the energy wasted in ohmic losses.

D. Self-Excited Operation

The search for differences between the models was carried out for the induction machine operating in self-excited generating mode, which is only possible in the magnetic saturation region. To perform the comparison, the responses of the SEIG around stable operating points are analyzed. The angular velocity of the generator is assumed to be constant, eliminating any effect from the mechanical transients.

Self-excited operation requires capacitors connected in parallel with the loads applied to the stator windings. Based on (1), the model of SEIG with resistive loads in the rotating reference frame *F–G* can be put into the following form [24]:

$$E\dot{X} = FX \tag{13}$$

where $X = [\,U_{\mathrm{SF}}\ i_{\mathrm{SF}}\ i_{\mathrm{RF}}\ U_{\mathrm{SG}}\ i_{\mathrm{SG}}\ i_{\mathrm{RG}}\,]^T$ and the matrices E and F attain the size 6×6 [24], additionally depending on the value of capacitor C and admittance of the resistive load $Y_L = 1/R_L$ (both added to each phase).

Combining (13) with (4) gives the alternative representation of the full SEIG model

$$E_L \dot{X} = FX - \frac{L - L_M}{i_M} \frac{di_M}{dt} X_M \tag{14}$$

where $X_M = [\,0\ i_{\mathrm{MF}}\ i_{\mathrm{MF}}\ 0\ i_{\mathrm{MG}}\ i_{\mathrm{MG}}\,]^T$, and E_L is of size 6×6 [24], additionally depending on C.

Then, the simplified nonlinear model of the SEIG is

$$E_L \dot{X} = FX. \tag{15}$$

The steady-state description of the SEIG is derived from (13), (14), or (15) taking $\dot{X} = 0$. Rearranging the steady-state model into a complex matrix form and exploiting properties of the matrix F [6] yield an explicit expression for the SEIG voltage magnitude $|U_S^*|$ as function of ω_e^*, L_M^*, and i_M^* for different Y_L and C, where the superscript "$*$" denotes steady-state values. The condition $\det(F^*) = 0$ [6] gives a polynomial of fifth order in ω_e^* whose solution gives the generated frequency and an explicit formula for the computation of the magnetizing inductance L_M^*. The value of i_M^* is determined from the descending part of the function $L_M = f_1(i_M)$.

E. Linearization of the Full Model

Linearization and analysis of both models are performed to predict differences in their transient behavior and to identify operating conditions where the difference will be most significant.

Linearization of (13) in the vicinity of an equilibrium X^* is carried out for small perturbations δX caused by small perturbations δC, δY_L, and $\delta\omega$, while neglecting perturbations of second-order and higher. The perturbation δL_M is found from the definition of the dynamic magnetizing inductance evaluated at X^*, whereas the perturbation $\delta\omega_e$ is eliminated from the model via alignment of the $F - G$ reference frame with the stator voltage vector (then, $U_{\mathrm{SF}}^* = |U_S^*|$, $U_{\mathrm{SG}}^* = 0$, $\delta U_{\mathrm{SF}} = \delta|U_S|$, and $\delta U_{\mathrm{SG}} = 0$). Following [25], the reduced-order linearized space-state description of the full model is obtained as

$$E^*\delta\dot{X} = (F^* + \delta F^* + F_{\omega e}^* F_{\omega eX}^*)\,\delta X + F_{\mathrm{YL}}^* \delta Y_L + F_{\omega e}^* F_{\omega eC}^* \delta C + F_{\omega}^* \delta\omega \tag{16}$$

where $\delta X = [\,\delta|U_S|\ \delta i_{\mathrm{SF}}\ \delta i_{\mathrm{RF}}\ \delta i_{\mathrm{SG}}\ \delta i_{\mathrm{RG}}\,]^T$, the matrices E^*, F^* and δF^* are of size 5×5 and F_{YL}^*, $F_{\omega eX}^{*\,T}$, $F_{\omega e}^*$, F_{ω}^* are vectors evaluated at the steady state [25]. All elements of δF^* are proportional to the difference $L^* - L_M^*$, $F_{\omega eC}^* = -\omega_e^*/C$.

Therefore, the equilibrium X^* is stable if and only if all the eigenvalues of the matrix

$$A^* = (E^*)^{-1}\,(F^* + \delta F^* + F_{\omega e}^* F_{\omega eX}^*) \tag{17}$$

are in the open left-half plane. The description allows one to obtain transfer functions from δC, δY_L, and $\delta\omega$ to $\delta|U_S|$. The difference between the full and simplified models will be most evident when the difference between their poles and zeroes is significant.

F. Linearization of the Simplified Model

The linearization of the simplified model is performed using a similar approach

$$E_L^*\delta\dot{X} = \left(F^* + \delta F^* + F_{\omega e}^* F_{\omega eX}^*\right)\delta X + F_{\mathrm{YL}}^*\delta Y_L + F_{\omega e}^* F_{\omega eC}^*\delta C + F_{\omega}^*\delta\omega, \quad (18)$$

where

$$E_L^* = \begin{bmatrix} E_{\mathrm{LM}}^* & N^T \\ N & E_{\mathrm{LM1}}^* \end{bmatrix},\ E_{\mathrm{LM}}^* = \begin{bmatrix} -C & 0 & 0 \\ 0 & L_{\sigma\mathrm{S}}+L_M^* & L_M^* \\ 0 & L_M^* & L_{\sigma\mathrm{R}}+L_M^* \end{bmatrix},$$

$$E_{\mathrm{LM1}}^* = \begin{bmatrix} L_{\sigma\mathrm{S}} + L_M^* & L_M^*; & L_M^* & L_{\sigma\mathrm{R}} + L_M^* \end{bmatrix},$$

$$N = \begin{bmatrix} 0\ 0\ 0; & 0\ 0\ 0 \end{bmatrix}.$$

System (18) differs from description (16) only by the matrix E_L^* replacing E^*. However, the system cannot be obtained from (16) with L^* replaced by L_M^*, as is the case for the original nonlinear models (this would mean that $\delta F^* = 0$). In the process of linearization, L^* actually reappears in the description of the simplified model. Note that, like the nonlinear models, the linearized systems predict the same steady-states since, with $\delta\dot{X} = 0$, (16) and (18) are identical.

G. Magnetizing Inductance Curve Determination

Because differences between the models are relatively small, it is important to minimize errors that could randomly favor one model over another. A precise determination of the magnetizing curve is particularly important in that regard. The curve was determined based on the "no load motor tests," and extended to the part of the curve most critical for the comparative simulations using the experimental SEIG steady-state voltages as functions of velocity and for different loads and capacitances. According to Section II-D, at first, the dependency of L_M^* on ω is found for given C and Y_L based on measured frequencies ω_e^*. Then, the corresponding values of i_M^* are computed using the measured voltages, ω_e^* and L_M^*.

III. Simulations and Experimental Results

A. Experimental Testbed

A three-phase induction motor (Bk2208, with rated values 250 W, 240 V (Δ), 50 Hz, and 1425 r/min) was used for experiments as SEIG. The following parameters of the generator were determined experimentally $R_S = 31.65\,\Omega$, $R_R = 28.1\,\Omega$, $L_{\sigma\mathrm{S}} = L_{\sigma\mathrm{R}} = 0.0921$ H, and $n_p = 2$.

The SEIG was coupled to another induction motor (M3AA090LB-4, with rated values 1.1 kW, 230 V (Δ), 50 Hz, and 1435 r/min) controlled through a frequency converter ABB ACS355 with rated power 1.1 kW feeding the stator windings. The higher value of the motor's power and the slip compensation function of the ACS355 provided some velocity stabilization during experiments.

Line-to-line voltage measurements were taken between all three phases through voltage transducers LV25-P and read through a dSPACE DS1104 data acquisition system.

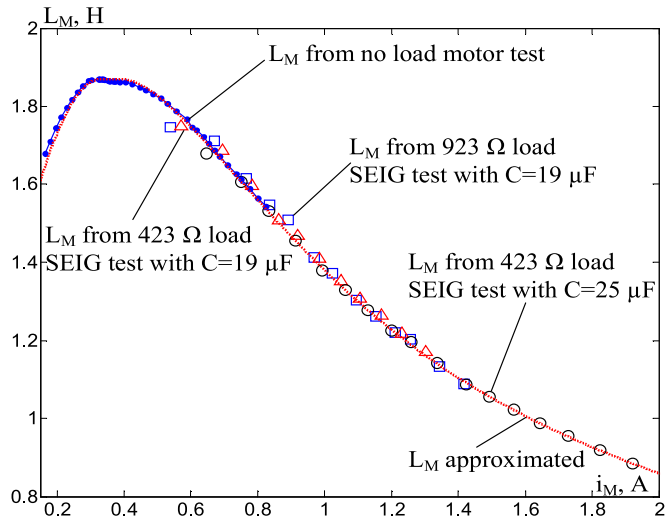

Fig. 1. Experimentally derived and analytic approximation of the extended magnetizing inductance curve.

Computational results obtained from the analysis of Section II were converted using a Y to Δ transformation to obtain line-to-line stator voltages. The excitation capacitors and the loads were Y-connected, and the values of load admittances and capacitances shown in the figures are actual values (i.e., line to neutral). The capacitors were engaged through three-phase relays controlled through DS1104 logical outputs and transistors switches. The velocity of the motor was monitored through an A2108 optical tachoprobe.

B. Experimental Extended Part of the Magnetizing Inductance Curve

Fig. 1 shows the function $L_M = f_1(i_M)$ computed based on the experimental data from the no load motor tests and extended using the data derived according to Section II-G from experimental steady-state SEIG curves. The analytic approximation of L_M is given in the appendix. The part of the approximation for lower currents was obtained iteratively through simulation of the voltage build-up based on the full nonlinear model, and comparing to the corresponding test data. Note that only the descending part of the $L_M = f_1(i_M)$ curve is used by the simulation for comparison of the full and simplified SEIG models.

C. SEIG Steady-State Characteristics

Fig. 2 shows the computed and experimental values of the line-to-line stator voltage magnitude $|U_{\mathrm{SL}}^*|$ as function of ω for different operating conditions. The absolute values of the steady-state errors for the velocity range from 160.14 to 188.4 rad/s (the frequency of the voltage feeding the prime mover from 51 to 60 Hz) remain approximately the same for the cases of 423 and 523 Ω loads with $C = 19\,\mu$F, meaning that these cases are suitable for the models comparison. The relative value of the error does not exceed 3% in these cases.

Similarly, the capacitance range from 19 to 25 μF was found suitable for the comparison in the case of a velocity

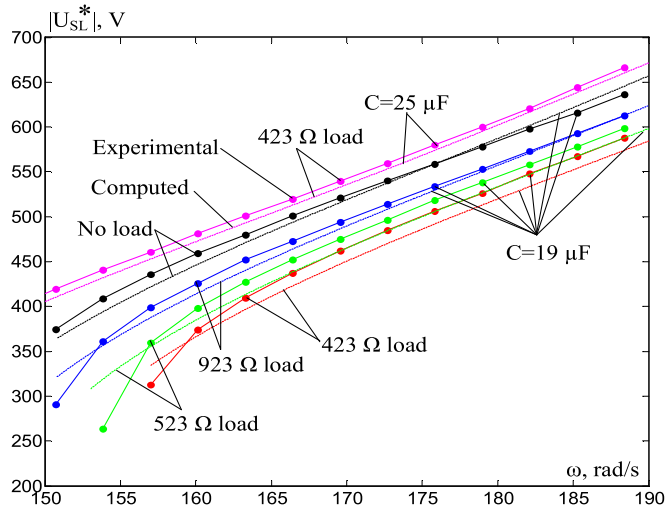

Fig. 2. Steady-state line-to-line voltage magnitude as a function of velocity for different capacitances and loads.

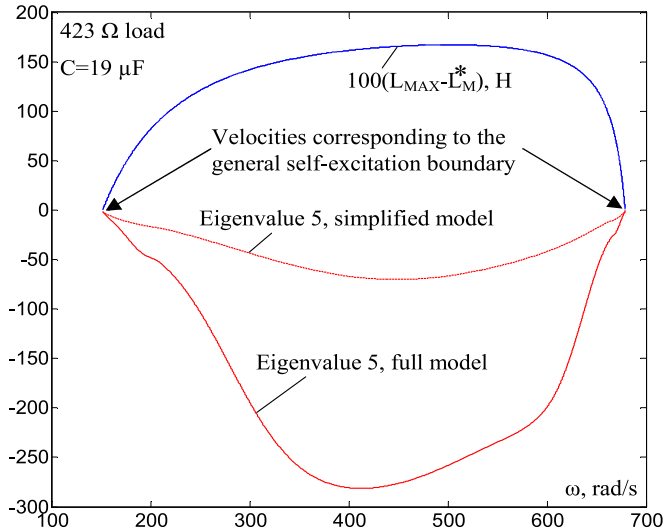

Fig. 3. Eigenvalues 5 as functions of the velocity for both linearized systems and corresponding to the descending part of the L_M curve.

of 160.14 rad/s with 423 or 523 Ω loads. The range of load admittance from 1/923 to 1/423 Ω^{-1} was also found suitable for the comparison for the cases of $C = 19,\ 21$, or 31 μF with $\omega = 160.14$ rad/s.

D. Computation of Eigenvalues

The eigenvalues of the linearized systems of both models were computed as functions of the velocity, capacitance and load admittance within the ranges corresponding to the general self-excitation boundaries, for the cases identified as suitable for the comparison of the models in Section III-C. Only equilibria corresponding to the descending part of the L_M curve were considered (since the other ones are unstable [6]). In all cases, the five eigenvalues for both systems always hold the following properties: four were a pair of complex conjugates with negative real parts and one was a nonzero negative real value. The complex eigenvalues were close for both systems, and were well into the stable side of the complex plane. The difference between the systems was determined mainly by the large difference in the real eigenvalue (referred to as #5).

For the case of varying velocity, the biggest difference between eigenvalues 5 of the linearized systems was in the middle of the general self-excitation boundaries. Fig. 3 reports the results of computations for the case of 423 Ω load and 19 μF capacitance. It was also observed that the real parts of the complex eigenvalues were comparable to the maximum real eigenvalue for the full model, which could hinder the comparison. Similar results were obtained for 523 Ω load and $C = 19$ μF. Eventually, the region from 160.14 to 188.4 rad/s was selected for the comparison, as it provides a significant difference between the eigenvalues 5 for both models, and a sufficient separation from the other complex eigenvalues.

Similar analyses confirmed that the conditions and the capacitance and load ranges determined in Section III-C were sufficient for the comparison tests.

In all the cases, the eigenvalues of both systems predict rapidly-decaying oscillations following by a slower exponentially decaying component. The initial oscillatory parts of the transients are hardly distinguishable between the models. However, the difference between the models could be easily observed for the exponential components since the simplified model predicts a slower response than the full model.

E. Transfer Functions

The state-space descriptions (16) and (18) yield transfer functions which differ only by the values of the parameters

$$P_\omega(s) = \frac{\delta\,|U_{\rm SL}|\,(s)}{\delta\omega(s)} = \frac{k_\omega(1+T_{\omega1}s)(1+2\zeta_\omega T_{\omega2}s+T_{\omega2}^2s^2)}{Z(s)}$$

$$P_C(s) = \frac{\delta\,|U_{\rm SL}|\,(s)}{\delta C(s)} = \frac{k_C(1+T_{C1}s)(1-T_{C2}s)(1+T_{C3}s)}{Z(s)}$$

$$P_{\rm YL}(s) = \frac{\delta\,|U_{\rm SL}|\,(s)}{\delta Y_L(s)} = \frac{D(s)}{Z(s)} \qquad (19)$$

where $Z(s) = (1+T_1s)(1+2\zeta_2T_2s+T_2^2s^2)(1+2\zeta_3T_3s+T_3^2s^2)$ and $D(s) = k_{\rm YL}(1+T_{\rm YL1}s)(1+T_{\rm YL2}s)(1+2\zeta_{\rm YL}T_{\rm YL3}s+T_{\rm YL3}^2s^2)$.

For the operating condition of $\omega = 160.14$ rad/s, $C = 19$ μF, and $Y_L = 1/423\,\Omega^{-1}$, the parameters for the full model are $T_{\omega1} = 27.3$ ms, $T_{\omega2} = 0.99$ ms, $\zeta_\omega = 0.227$, $T_1 = 101.3$ ms, $T_2 = 1.47$ ms, $\zeta_2 = 0.372$, $T_3 = 0.792$ ms, $\zeta_3 = 0.16$, $T_{C1} = 6$ ms, $T_{C2} = 1.5$ ms, $T_{C3} = 0.866$ ms, $T_{\rm YL1} = 19.7$ ms, $T_{\rm YL2} = 3.18$ ms, $T_{\rm YL3} = 0.99$ ms, $\zeta_{\rm YL} = 0.213$. The parameters of the simplified model are $T_{\omega1} = 42.9$ ms, $T_{\omega2} = 1$ ms, $\zeta_\omega = 0.235$, $T_1 = 163.1$ ms, $T_2 = 1.45$ ms, $\zeta_2 = 0.362$, $T_3 = 0.803$ ms, $\zeta_3 = 0.165$, $T_{C1} = 7.6$ ms, $T_{C2} = 1.8$ ms, $T_{C3} = 0.928$ ms, $T_{\rm YL1} = 31.1$ ms, $T_{\rm YL2} = 3.16$ ms, $T_{\rm YL3} = 1$ ms, $\zeta_{\rm YL} = 0.222$. The gains of both transfer functions are the same and equal to $k_\omega = 9.84$ V/(rad/s), $k_{\rm YL} = -43.4\cdot10^3$ V/Ω^{-1}, $k_C = 32$ V/μF The largest difference

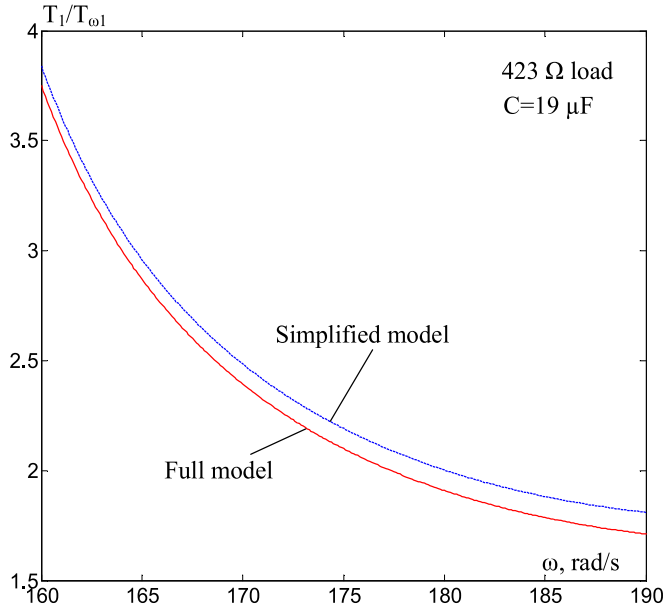

Fig. 4. Ratios of T_1 to $T_{\omega 1}$ computed through a range of velocity.

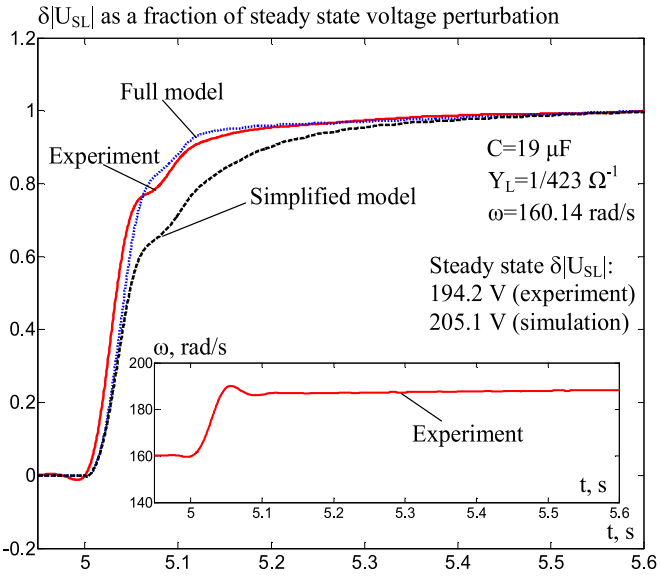

Fig. 5. Comparison of the models for velocity increase.

between the corresponding parameters is for the large time constant T_1, which was expected from the analysis of Section III-D. For the numerators of the transfer functions, the largest difference is for $T_{\omega 1}$, T_{C1}, and $T_{\mathrm{YL}1}$, which are the second biggest time constants in the corresponding transfer functions. However, the ratios of T_1 to $T_{\omega 1}$, T_{C1}, and $T_{\mathrm{YL}1}$ obtained for corresponding linearized systems are quite close. Similar properties hold for the whole corresponding self-excitation boundaries. Fig. 4 shows the computed ratios of T_1 to $T_{\omega 1}$ for the range of velocities chosen for the models comparison. The difference between the ratios does not exceed 3% with respect to the highest ratio for the full model within this range. For the range of capacitance from 19 to 25 μF, $\omega = 160.14$ rad/s, and 423 Ω load, the maximum difference for T_1/T_{C1} is 16%. For the range of loads from 423 to 923 Ω, $\omega = 160.14$ rad/s and $C = 31$ μF, the highest difference between $T_1/T_{\mathrm{YL}1}$ is 6%.

It was also observed that the so-called high-frequency gains of the transfer functions obtained as $\lim_{s\to\infty} P_C(s)$ and $\lim_{s\to\infty} P_{\mathrm{YL}}(s)$ were the same for both linearized systems within the corresponding self-excitation boundaries. The difference between the gains $\lim_{s\to\infty} P_\omega(s)$ did not exceed 0.05% within the velocity range chosen for the comparison, and was up to 30% otherwise.

The significance of this observation is that the initial parts of the transients caused by step changes of ω, C, or Y_L would be hardly distinguishable between the models. Since the steady-state responses are supposed to be the same, any difference between the models can only be seen clearly in the middle of transients. An interpretation of this fact is that the initial response is dominated by a change of flux in the leakage inductances, whereas the steady-state response is determined by the magnetizing inductance, both of which are identical for both models.

F. Simulation of Voltage Perturbations and Experiments

The comparison of the models is performed based on the simulation of the stator voltage amplitude deviations caused by the step changes of the velocity, capacitance, or load within the ranges and for the conditions determined in Sections III-C and III-D. Because the amplitudes of both simulated and measured voltages are close, variations $\delta|U_{\mathrm{SL}}| = |U_{\mathrm{SL}}| - |U^*_{\mathrm{SL}}|$ with respect to the steady-state are considered for enhanced visualization and closer inspection. To account for mechanical transients present in the real system and remove a potential source of bias, measured values of angular velocity are incorporated into simulations instead of preset step change or constant values.

The comparison was made for the case of the initial steady-state with $C = 19\,\mu$F, $Y_L = 1/423\,\Omega^{-1}$, and $\omega = 160.14$ rad/s perturbed by the "step" change of the velocity $\delta\omega = 28.26$ rad/s at $t = 5$ s. The simulated behaviors of both models were quite close to the experimental results. It was noticed that the steady-state errors were of the same order of magnitude as the difference between the models. To remove the steady-state voltage errors from the comparison, the voltage perturbation curves are plotted in Fig. 5 as fractions of the corresponding steady-state perturbations, which shows clearly that the full model predicts more accurately the settling time and the shape of the voltage response curve. The transients caused by the return of the velocity from 188.4 rad/s to its initial value of 160.14 rad/s also distinctly favored the full model over the simplified model. The same tests for the case of $C = 19\,\mu$F and 523 Ω load led to similar conclusions with a clear preference for the full model.

The results for the case of a capacitance step change are presented in Fig. 6. During the transients, there is also a velocity disturbance caused by the torque change and the slow response of the slip compensation system of the converter feeding the prime mover. The difference between the simulated and experimental initial negative voltage perturbation spikes just after $t = 5$ s is because the models assume that the engaging

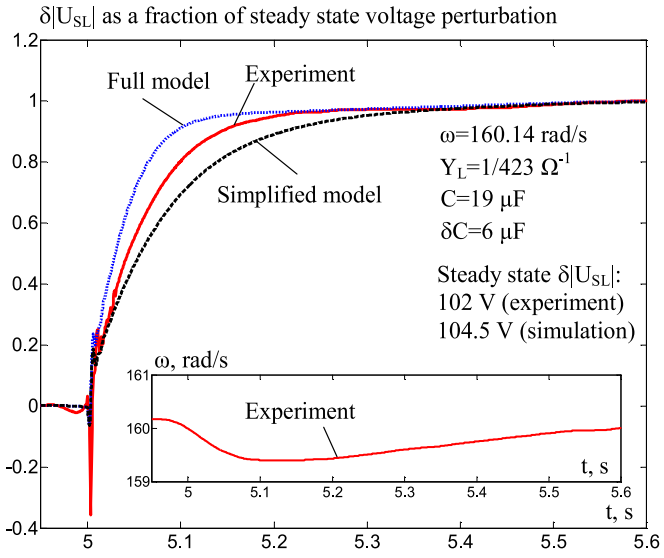

Fig. 6. Comparison of the models for capacitance increase.

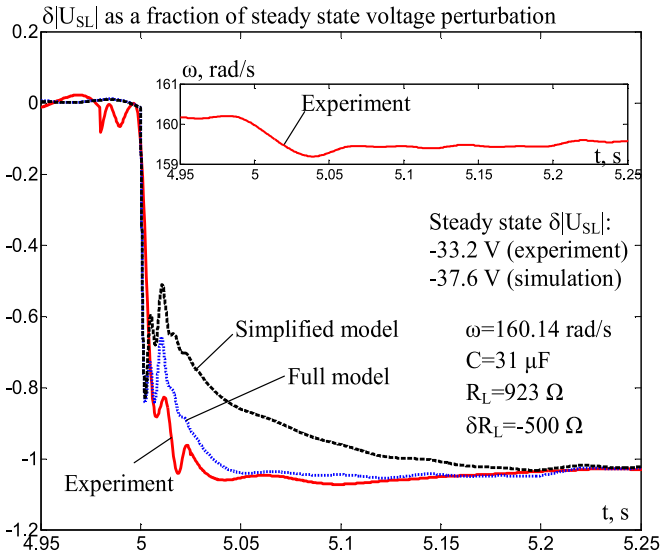

Fig. 7. Comparison of the models for load increase.

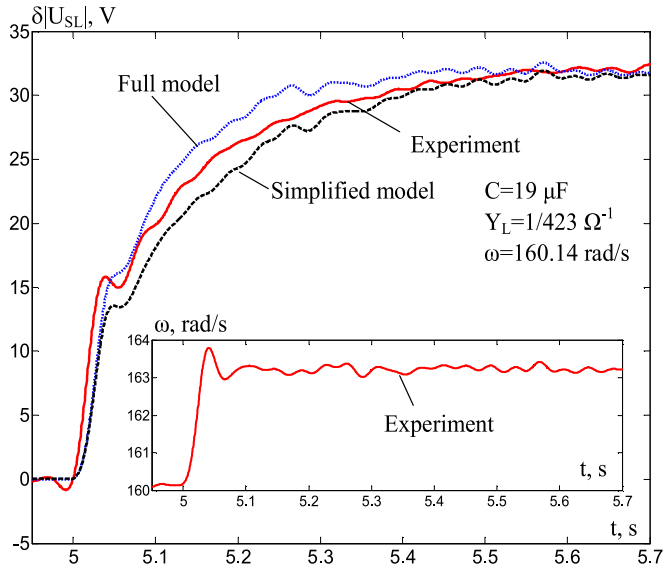

Fig. 8. Comparison of the models for small velocity increase.

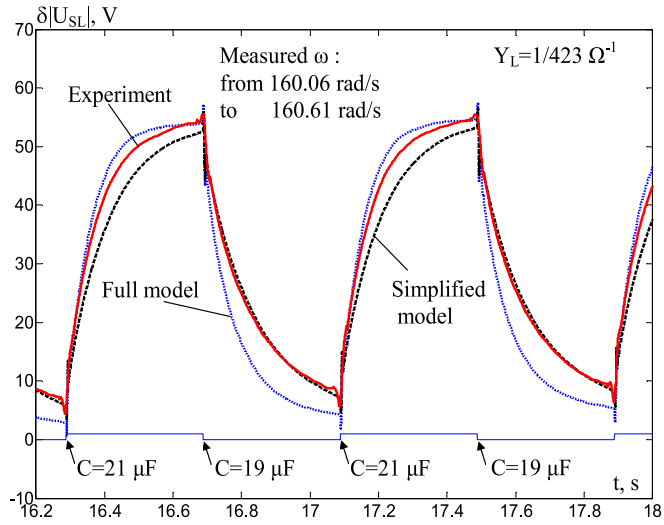

Fig. 9. Comparison of the models for small periodic capacitance change.

capacitors voltages and the stator voltages are the same. The accuracy of the full model is seen to be a bit higher than that of the simplified model.

The investigation of the transients for capacitance decrease from 25 to 19 μF also confirmed the higher accuracy of the full model. Similar conclusions were confirmed for a different operating point with 160.14 rad/s and 523 Ω load.

The results of the voltage deviations as results of the load increase from 923 to 423 Ω (see Fig. 7) also show the expected difference between the models. The same results were observed for the load decrease from 423 to 923 Ω, and for similar experiments with 19 and 21 μF capacitors.

The experiments above were performed for large enough perturbations to bring the operating point deep into the saturated region. When the SEIG operation remained close to the corresponding self-excitation boundaries, no clear evidence was found about which model was more accurate. The research was carried out for the initial conditions of Fig. 5 with the velocity perturbation of 3.14 rad/s (see Fig. 8). Accuracy of the simulation was improved through linear approximation of the L_M curve for the required magnetizing current region based on the experimental data for the initial and final operating points according to Section II-G. This provided almost zero steady-state errors for both initial and final operating points. As a result, there was no need to make the comparison based on the fractions of the corresponding steady-state perturbation.

Similar results were obtained for the condition of Fig. 6 with a capacitance step increase of 2 μF, and for the following return from $C = 21$ to 19 μF.

Further, a periodic switching of the capacitance between 19 and 21 μF was investigated, not allowing the voltage to reach the corresponding steady state (see Fig. 9). As expected, the amplitude of the voltage perturbation oscillations is lower for

the simplified model. However, there is no phase shift introduced due to slower exponential decaying component of the simplified model because of the same high-frequency gains of the models and very close ratios of T_1/T_{C1}, meaning that the error of the simplified model does not accumulate over the period of the transient. Voltage oscillations without reaching steady-states caused by periodic velocity change between 160.14 and 163.28 rad/s were also investigated for $C = 19\,\mu$F and $Y_L = 1/423\,\Omega^{-1}$, yielding similar conclusions.

IV. Conclusion

This paper provided clear evidence that the full nonlinear model of the induction machine accounting for magnetic saturation is more accurate than the simplified model ignoring the dynamic cross-saturation effect. The difference between the models was visible during transients deep into the saturated region. However, in many cases, the difference was not evident due to the inaccuracy of the models' parameters and, possibly, inaccuracy of the full model itself. For realistic operation slightly within the saturated region, the difference between the models was rather small. Linearization of the models for the self-excited generating mode in the reference frame aligned with the stator voltage vector yielded the same transfer functions relating the stator voltage magnitude to various perturbations, but with different parameters. However, many parameters remained the same, including steady-state and high-frequency gains, and some ratios of significant time constants in the numerator and denominator polynomials were very close. Therefore, despite significant differences in a dominant pole, the difference between the models during SEIG step responses could only be seen clearly in the middle of the transients. Regardless of a questionable theoretical basis for the simplified model, the responses it provides constituted a very good approximation of the more complex model. An open question, though, is whether the use of the models for the design of voltage controllers could enhance the difference between the models.

Appendix
Analytic Approximation of Magnetizing Inductance Curve

To facilitate simulations, an analytic approximation of the magnetizing inductance curve obtained experimentally was used. Four regions were defined, with breakpoints i_{M1}, i_{M2}, and i_{M3}:

1) For $i_M < i_{M1}$ (the ascending part of the L_M curve),

$$L_M = L_{\mathrm{MAX}} - b_1 (i_M - i_{M1})^2 \tag{20}$$

where L_{MAX} is a maximum (unsaturated) value of L_M. If $L_M(0) = L_{M0}, b_1 = (L_{\mathrm{MAX}} - L_{M0})/i_{M1}^2$.

2) For $i_{M1} < i_M < i_{M2}$ (the flat part), $L_M = L_{\mathrm{MAX}}$.

3) For $i_{M2} < i_M < i_{M3}$ (the descending part of L_M curve),

$$L_M = p_1 i_M^3 + p_2 i_M^2 + p_3 i_M + p_4 + p_5 i_M^{-1}. \tag{21}$$

4) For $i_M > i_{M3}$,

$$L_M = \left(\Psi_{\mathrm{MMAX}} - (\Psi_{\mathrm{MMAX}} - \Psi_{M3})\, e^{-(i_M - i_{M3})/i_D}\right)/i_M \tag{22}$$

where $\Psi_{M3} = p_1 i_{M3}^4 + p_2 i_{M3}^3 + p_3 i_{M3}^2 + p_4 i_{M3} + p_5$.

From experimental data, the parameters were determined to be: $L_{\mathrm{MAX}} = 1.87$ H, $L_{M0} = 1$ H, $i_{M1} = 0.333$ A, $i_{M2} = 0.401$ A, $b_1 = 7.8457$ H/A^2, $i_{M3} = 1.738$ A, $\Psi_{\mathrm{MMAX}} = 2.05$ Wb, $p_1 = -0.2116$ H/A^3, $p_2 = 1.33$ H/A^2, $p_3 = -3.203$ H/A, $p_4 = 3.807$ H, $p_5 = -0.342$ HA, $i_D = 1.411$ A.

References

[1] E. Levi, "A unified approach to main flux saturation modeling in d-q axis models of induction machines," *IEEE Trans. Energy Convers.*, vol. 10, no. 3, pp. 455–461, Sep. 1995.

[2] E. Levi, "Main flux saturation modeling in double-cage and deep-bar induction machines," *IEEE Trans. Energy Convers.*, vol. 11, no. 2, pp. 305–311, Jun. 1996.

[3] I. R. Smith and S. Sriharan, "Transients in induction machines with terminal capacitors," *Proc. IEE*, vol. 115, no. 4, pp. 519–527, Apr. 1968.

[4] K. P. Kovacs, *Transient Phenomena in Electrical Machines*, Budapest, Hungary: Academiai Kiado, 1984.

[5] K. P. Kovacs and L. Kiss, "Accurate simulation of a variable saturation asynchronous motor (Genaue Simulierung eines Asynchronmotors mit veraenderlicher Saettigung)," *Bull. Schweiz. Elektrotech.*, vol. 72, no. 13, pp. 671–673, Jul. 1981.

[6] M. Bodson and O. Kiselychnyk, "Analysis of triggered self-excitation in induction generators and experimental validation," *IEEE Trans. Energy Convers.*, vol. 27, no. 2, pp. 238–249, Jun. 2012.

[7] P. Vas, K. E. Hallenius, and J. E. Brown, "Cross-saturation in smooth-air-gap electrical machines," *IEEE Trans. Energy Convers.*, vol. EC-1, no. 1, pp. 103–112, Mar. 1986.

[8] Z. Krzeminski, "Differential equations of induction motor with nonlinear control synthesis with regard to saturation of main magnetic path," *Rozprawy Elektrotech.*, vol. 34, no. 1, pp. 117–131, 1988.

[9] E. Levi and Z. Krzeminski, "Main flux-saturation modelling in d-q axis models of induction machines using mixed current-flux state-space models," *Eur. Trans. Electr. Power*, vol. 6, no. 3, pp. 207–215, May/Jun. 1996.

[10] E. Levi, "Applications of the current state space model in analyses of saturated induction machines," *Elect. Power Syst. Res.*, vol. 31, no. 3, pp. 203–216, Dec. 1994.

[11] K.-E. Hallenius, P. Vas, and J. E. Brown, "The analysis of a saturated self-excited asynchronous generator," *IEEE Trans. Energy Convers.*, vol. 6, no. 2, pp. 336–345, Jun. 1991.

[12] C. Grantham, D. Sutanto, and B. Mismail, "Steady-state and transient analysis of self-excited induction generators," *IEE Proc. B, Elect. Power Appl.*, vol. 136, no. 2, Mar. 1989, pp. 61–68.

[13] L. Wang and C.-H. Lee, "A novel analysis on the performance of an isolated self-excited induction generator," *IEEE Trans. Energy Convers.*, vol. 12, no. 2, pp. 109–117, Jun. 1997.

[14] D. Seyoum, C. Grantham, and F. Rahman, "The dynamic characteristics of an isolated self-excited induction generator driven by a wind turbine," *IEEE Trans. Ind. Appl.*, vol. 39, no. 4, pp. 936–944, Jul./Aug. 2003.

[15] J. K. Chatterjee, B. V. Perumal, and N. R. Gopu, "Analysis of operation of a self-excited induction generator with generalized impedance controller," *IEEE Trans. Energy Convers.*, vol. 22, no. 2, pp. 307–315, Jun. 2007.

[16] K. L. V. Iyer, L. Xiaomin, Y. Usama, V. Ramakrishnan, and N. C. Kar, "A twofold Daubechies-wavelet-based module for fault detection and voltage regulation in SEIGs for distributed wind power generation," *IEEE Trans. Ind. Electron.*, vol. 60, no. 4, pp. 1638–1651, Apr. 2013.

[17] K. Hafiz, G. Nanda, and N. C. Kar, "Performance analysis of aluminum- and copper-rotor induction generators considering skin and thermal effects," *IEEE Trans. Ind. Electron.*, vol. 57, no. 1, pp. 181–192, Jan. 2010.

[18] B. Singh, S. S. Murthy, and S. Gupta, "STATCOM-based voltage regulator for self-excited induction generator feeding nonlinear loads," *IEEE Trans. Ind. Electron.*, vol. 53, no. 5, pp. 1437–1452, Oct. 2006.

[19] J. E. Brown, K. P. Kovacs, and P. Vas, "A method of including the effects of main flux path saturation in the generalized equations of A.C. machines," *IEEE Trans. Power App. Syst.*, vol. PAS-102, no. 1, pp. 96–103, Jan. 1983.

[20] E. Levi, "Impact of cross-saturation on accuracy of saturated induction machine models," *IEEE Trans. Energy Convers.*, vol. 12, no. 3, pp. 211–216, Sep. 1997.
[21] A. Campeanu, A. Ionescu, I. Vlad, and S. Enache, "Modeling and simulation of magnetic saturation in induction motors," in *Proc. IEEE Int. Electr. Mach. Drives Conf.*, 2007, pp. 688–693.
[22] A. Campeanu, M. Radulescu, I. Vlad, and S. Enache, "Influence of cross-saturation for modeling and simulation of the dynamic processes in the induction motor," in *Proc. Int. Conf. "Computer as a Tool*," Warsaw, Poland, 2007, pp. 1830–1833.
[23] *PLECS: The Simulation Platform for Power Electronics Systems. User Manual Version 3.7*, Plexim GmbH, Zurich, Switzerland, 2002–2015. [Online]. Available: http://www.plexim.com/sites/default/files/plecsmanual.pdf
[24] M. Bodson, O. Kiselychnyk, and J. Wang, "Comparison of two magnetic saturation models of induction machines," in *Proc. IEEE Int. Elect. Mach. Drives Conf.*, Chicago, IL, USA, 2013, pp. 1004–1009.
[25] O. Kiselychnyk, M. Bodson, and J. Wang, "Linearized state-space model of a self-excited induction generator suitable for the design of voltage controllers," *IEEE Trans Energy Convers.*, vol. 30, no. 4, pp. 1310–1320, Dec. 2015.
[26] P. C. Krause, O. Wasynczuk, and S. D. Sudhoff, *Analysis of Electric Machinery and Drive Systems*, 2nd ed. New York, NY, USA: Wiley, 2002.

Oleh Kiselychnyk (M'15) received the M.Sc. and Ph.D. degrees in electrical engineering and automation from the National Technical University of Ukraine "Kiev Polytechnic Institute" (NTUU "KPI"), Kiev, Ukraine, in 1993 and 1997, respectively.

He is currently an Assistant Professor in the School of Engineering, University of Warwick, Coventry, U.K. From 2012 to 2015, he was a Science City Research Fellow with the University of Warwick. Before 2012, he was a Docent in the Department of Electric Drives, NTUU "KPI". He was also a Visiting Fulbright Scholar with the University of Utah, Salt Lake City, UT, USA, in 2009, and a Visiting German Academic Exchange Service Researcher with the Hamburg University of Technology, Hamburg, Germany, in 2008. His main research interests include control of electric motors and generators, automation of water supply systems, and microcontrollers.

Marc Bodson (F'06) received the Ph.D. degree in electrical engineering and computer science from the University of California, Berkeley, CA, USA, in 1986, and two M.S. degrees, one in electrical engineering and computer science and the other in aeronautics and astronautics, from the Massachusetts Institute of Technology, Cambridge, MA, USA, in 1982.

He is currently a Professor of electrical and computer engineering with the University of Utah, Salt Lake City, UT, USA. Between July 2003 and October 2009, he was the Chair of the Department of Electrical and Computer Engineering . His research interests include adaptive control, with applications to electromechanical systems and aerospace.

Dr. Bodson was the Editor-in-Chief of the IEEE TRANSACTIONS ON CONTROL SYSTEMS TECHNOLOGY between January 2000 and December 2003.

Jihong Wang (M'06–SM'09) received the B.E. degree in electrical engineering from the Wuhan University of Technology, Wuhan, China, the M.Sc. degree in electrical engineering from the Shandong University of Science and Technology, Shandong, China, and the Ph.D. degree in control system theory from Coventry University, Coventry, U.K., in 1982, 1985, and 1995, respectively.

She is currently a Professor of power systems and control engineering with the School of Engineering, University of Warwick, Coventry, U.K. Her main research interests include nonlinear system control, system modeling and identification, power systems, energy-efficient systems and actuators, and applications of intelligent algorithms.